Published OnlineFirst March 6, 2019; DOI: 10.1158/0008-5472.CAN-18-1421

Metabolism and Chemical Biology

Cancer Research

Stabilized Peptide HDAC Inhibitors Derived from HDAC1 Substrate H3K56 for the Treatment of Cancer Stem–Like Cells *In Vivo*

Dongyuan Wang[1], Wenjun Li[1], Rongtong Zhao[1], Longjian Chen[1], Na Liu[1], Yuan Tian[2], Hui Zhao[3], Mingsheng Xie[1], Fei Lu[1], Qi Fang[1], Wei Liang[4], Feng Yin[1], and Zigang Li[1]

Abstract

FDA-approved HDAC inhibitors exhibit dose-limiting adverse effects; thus, we sought to improve the therapeutic windows for this class of drugs. In this report, we describe a new class of peptide-based HDAC inhibitors derived from the HDAC1-specific substrate H3K56 with improved nonspecific toxicity compared with traditional small-molecular inhibitors. We showed that our designed peptides exerted superior antiproliferation effects on cancer stem–like cells with minimal toxicity to normal cells compared with the small-molecular inhibitor SAHA, which showed nonspecific toxicity to normal and cancer cells. These peptide inhibitors also inactivated cellular HDAC1 and HDAC6 and disrupted the formation of the HDAC1, LSD1, and CoREST complex. In ovarian teratocarcinoma (PA-1) and testicular embryonic carcinoma (NTERA-2) cell xenograft animal models (5 mice/group, 50 mg/kg, every other day, intraperitoneal injection), these peptides inhibited tumor growth by 80% to 90% with negligible organ (heart, liver, spleen, lung, kidney, brain) lesions. These results represent the first attempt to design chemically stabilized peptide inhibitors to investigate HDAC inhibition in cancer stem–like cells. These novel peptide inhibitors have significantly enhanced therapeutic window and offer promising opportunities for cancer therapy.

Significance: Selective antiproliferative effects of stabilized peptide HDAC inhibitors toward cancer stem–like cells provide a therapeutic alternative that avoids high nonspecific toxicity of current drugs.

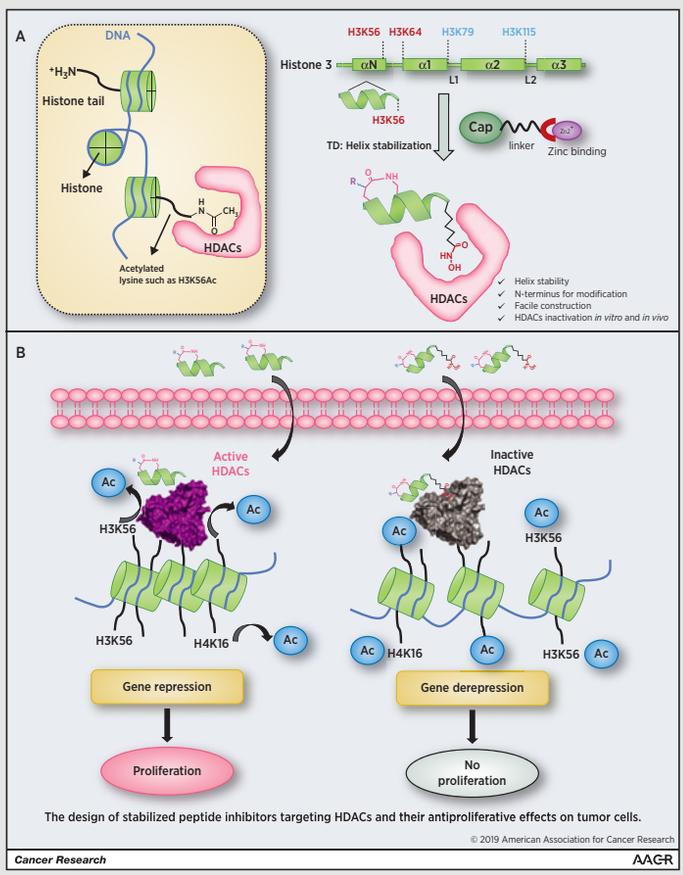

Graphical Abstract: http://cancerres.aacrjournals.org/content/canres/79/8/1769/F1.large.jpg.

[1]School of Chemical Biology and Biotechnology, Peking University Shenzhen Graduate School; State Key Laboratory of Chemical Oncogenomics, Key Laboratory of Chemical Genomics, Peking University Shenzhen Graduate School, Shenzhen, China. [2]School of Life Science and Engineering, Southwest Jiaotong University, Chengdu, China. [3]Division of Life Science, Clarivate Analytics, Beijing, China. [4]Department of Radiation Oncology, The First Affiliated Hospital, Anhui Medical University, Hefei, China.

Note: Supplementary data for this article are available at Cancer Research Online (http://cancerres.aacrjournals.org/).

Corresponding Authors: Zigang Li, Peking University, Shenzhen 518055 China. Phone: 755-26033616; E-mail: lizg@pkusz.edu.cn; and Feng Yin, School of Chemical Biology and Biotechnology, Peking University Shenzhen Graduate School, Shenzhen University Town, Lishui Road, Xili Town, Nanshan District, Shenzhen,China. Phone: 755-26033611; E-mail: yinfeng@pkusz.edu.cn

doi: 10.1158/0008-5472.CAN-18-1421

©2019 American Association for Cancer Research.

Downloaded from cancerres.aacrjournals.org on August 7, 2019. © 2019 American Association for Cancer Research.

Published OnlineFirst March 6, 2019; DOI: 10.1158/0008-5472.CAN-18-1421

Introduction

Two of the most fundamental hallmarks of malignant tumors are their heterogeneous nature and limitless proliferation potential (1). The cancer stem cell (CSC) theory states that malignant proliferation can be fueled by a small subset of stem-like tumor cells, which possess similar properties as typical stem cells and can contribute to drug resistance and cancer relapse (2). Cancer stem–like cells have been found in many common cancer types such as breast cancer (3), colorectal cancer (4), ovarian cancer (5), and lung cancer (6). Increasing evidence has revealed that epigenetic mediators, especially HDACs, can contribute to the emergence and maintenance of CSCs (7–9). HDACs control cancer cell fortune through the removal of the acetyl group of histone and nonhistone proteins. The aberrant acetylation of histones has been identified in oncogenesis, for example, the loss of acetylation of H4K16 (H4K16ac) is found in various cancer types such as lymphoma, and cancers of the breast, colon, and lung (10). Additionally, HDACs can interact directly with some transcription factors, such as E2F, Stat3, p53, Rb, and NF-κB, to regulate important signaling pathways (11). Thus, the aberration of HDACs in cancer cells has fueled intense interest in the development of HDAC inhibitors for cancer therapy (12).

HDACs are grouped into four classes based on their homology: class I (HDACs 1, 2, 3, and 8), class II (HDACs 4–7, 9, and 10), and class IV (HDAC 11) are Zn^{2+} dependent, and class III, referred to as sirtuins, are NAD^{+} dependent (13). Different HDACs are thought to have their own substrate specificity, including histone substrates and nonhistone substrates. However, the identification of their histone substrates is difficult as different HDACs or HDAC complexes may have synergistic effects (14). Nowadays, HDAC1 is reported to have preference for H3K56ac and H4K16ac, while HDAC3 preferentially deacetylates H4K5 and H4K12 (14–16). For nonhistone substrates, HDAC1 and Sirtuin 1 are reported to deacetylate P53 (17, 18), and HDAC6 is reported to deacetylate lysine 40 of α-tubulin (19).

Due to the high similarity of the Zn^{2+}-dependent enzyme pockets of HDACs, the four FDA-approved drugs are all pan-HDAC inhibitors and usually share a common dose-limiting toxicity, impeding their further clinical application (20). The intrinsic biocompatibility and complex chemical structure of peptides have attracted chemists to develop peptide inhibitors with improved HDAC isoform selectivity. The most famous peptide-based HDAC inhibitors are cyclic tetrapeptides equipped with active Zn^{2+} binding groups, such as the approved drug FK228 (21). These macrocyclic peptides usually display class I selectivity, and the selectivity is hypothesized to be attributed to peptide complex cap groups that interact with a large area of the enzyme surface (22). Despite its preference for class I HDACs, FK228 still shows the common side effects of other approved HDACIs. Thus, it is still unclear whether or not an isoform-selective HDAC inhibitor would be advantageous over pan-HDAC inhibitors in cancer therapy (20). Therefore, taking the peptides' biocompatibility and affinity for target binding into consideration, we hypothesized that a suitable HDAC-interacting peptide bearing an active Zn^{2+} binding group might provide a suitable scaffold for novel HDACIs, which would result in a significantly increased safety window and better selectivity toward malignant cells.

Peptidomimetics are efficient tools to inhibit protein–protein interactions and have emerged as a new modality for cancer therapy. Recently, our group has developed several efficient helical stabilization methodologies including the N-terminal helix nucleating template (TD strategy) and the in-tether chiral center induced peptide helicity (CIH strategy) based on the concept that a precisely tuned in-tether chiral center could dominate the peptide's secondary structure and its biological functions (23, 24). Peptides constructed with these methods are successfully utilized to target ERα–coactivator interaction and p53–MDM2/MDMX interaction (25, 26). Inspired by the previous success of FK228 and our own experience in stabilized peptides, we hypothesized that peptide substrate analogues with large binding surfaces could achieve enhanced efficiency and reduced toxicity through effectively disrupting the interaction between HDACs and their substrates. The HDAC substrates acetylated H3K56 and H4K16 have been reported to have a preference for HDAC1 and were previously examined (15, 16). Thus, we chose to modify the helical region (comprising residues 45–56) of H3 and stabilized the peptide structure using our developed method—the TD strategy. We envisioned that these stabilized peptide-based HDAC inhibitors with large interacting interfaces could improve the molecules' selectivity for HDACs over other nonspecific interacting proteins and ultimately reduce nonspecific toxicity. In this report, we found the designed peptide inhibitors showed potent pan-HDAC inhibition but selective cytotoxicity toward cancer stem–like cells (PA-1 cells and NTERA-2 cells) along with negligible toxicity toward normal cells even at much higher concentrations. The superior tumor-inhibiting effect displayed in the PA-1 and NTERA-2 xenograft animal models resulted in negligible organ lesions at the high dosage (50 mg/kg, every other day), further supporting the efficiency and safety of our designed peptides. To our knowledge, this study was the first to showcase the stabilized peptide as a cap group used to decrease the nonspecific toxicity of HDAC inhibitors, demonstrating the wide potential for combined application of stabilized peptides with clinical approved therapeutics.

Materials and Methods

Materials

All solvents and reagents used for solid-phase peptide synthesis were purchased from Shanghai Hanhong Chemical Co., J&K Co. Ltd., Shenzhen Tenglong Logistics Co., or Energy Chemical Co. and were used without further purification unless otherwise stated. Antibodies against HDAC6, HDAC8, P21 Sox2, Ac-tubulin, GAPDH, and H3 were obtained from Proteintech; antibodies against histone H4K16ac were obtained from Millipore; antibodies against HDAC1, HDAC4, HDAC5, SIRT6, LSD1, H3K4m1, H3K4me2, H4, and active caspase-3 were obtained from Abcam; antibodies against HDAC2 and HDAC3 were obtained from BETHYL; antibody against H3K56ac was obtained from Millipore and Active motif. The purified recombinant human HDAC 3, 6, 8 and their corresponding substrates were purchased from BioVision Inc. The purified recombinant human HDAC1 was obtained from Caymanchem Inc. Annexin V: FITC Apoptosis Detection Kit I was obtained from BD Pharmingen. Reagents used for biological assays were purchased from Sigma-Aldrich and Thermo Fisher. Cells were purchased through ATCC and cultured according to ATCC guidelines.

Tumor cell lines and culture

Human ovarian cancer cell lines, PA-1 cells (CRL-1572, ATCC, 2018), were cultured in MEM with 10% (v/v) fetal bovine serum (FBS) and penicillin/streptomycin (100 g/mL). Human

Downloaded from cancerres.aacrjournals.org on August 7, 2019. © 2019 American Association for Cancer Research.

Published OnlineFirst March 6, 2019; DOI: 10.1158/0008-5472.CAN-18-1421

malignant pluripotent embryonal carcinoma, NTERA-2 cells (CRL-1973, ATCC, 2018), were cultured in DMEM with 10% (v/v) FBS and penicillin/streptomycin (100 g/mL). Human lung adenocarcinoma, A549 cells (CCL-185, ATCC, 2018), were cultured in RPMI-1640 supplemented with 10% (v/v) FBS and penicillin/streptomycin (100 g/mL). Human cervix adenocarcinoma, HeLa cells (CCL-2, ATCC, 2018), and human kidney cells, 293T (CRL-11268, ATCC, 2018), were cultured in DMEM with 10% (v/v) FBS and penicillin/streptomycin (100 g/mL). Chang liver cells (gifts from the South China University of Technology) were cultured in DMEM with 10% (v/v) FBS and penicillin/streptomycin (100 g/mL). All reagents were purchased from Gibco. All these cells were maintained in a humidified incubator containing 5% CO_2 at 37°C. All cells were authenticated at the Nevada Cancer Institute by specific markers such as Oct4, Sox2, p53, and $p16^{Ink4a}$ and by their cell morphology and used within 3 months.

Peptide synthesis

Details of the syntheses of peptide inhibitors and their structure analysis were given in the Supplementary Methods.

In vitro deacetylation assays

The purified recombinant human HDAC 3, 6, 8 and their corresponding substrates were purchased from BioVision Inc. The purified recombinant human HDAC1 was obtained from Caymanchem Inc. as the unavailable source from BioVision Inc. HeLa nuclear extract was obtained according to the Nuclear Extraction Kit (Solarbio). Assays were carried out in 384-well format using the fluorometric histone deacetylase kit according to the manufacturer's protocol (BioVision and Caymanchem). HDAC activity was detected at the excitation wavelength of 360 nm and the emission wavelength of 460 nm using Envision (PerkinElmer). The analytical software, GraphPad Prism 5.0 (GraphPad Software, Inc.) was used to generate IC_{50} value via nonlinear regression analysis.

Cell viability assay

Cell viability for different cell lines was measured by MTT (3-(4, 5-dimethylthiazol-2-yl)-2, 5-diphenylt-etrazolium bromide, from Sigma) assays. The cells were incubated on a 96-well plate for 24 hours in growth medium prior to drug treatment. Then the media were removed followed by adding peptides or suberoylanilide hydroxamic acid (SAHA) in medium with 5% FBS (v/v) for 24-hour incubation, replaced by 10% FBS medium for another 24 hours, if necessary. MTT (5 mg/mL, 20 μL) in phosphate-buffered saline (PBS) was added, and the cells were incubated for 4 hours at 37°C with 5% CO_2. DMSO (150 μL, Sigma) was then added to solubilize the precipitate with 10 minutes of gentle shaking. Absorbance was measured with a microplate reader (Bio-Rad) at a wavelength of 490 nm.

Western blot

For Western blot analysis, different cancer cells were seeded in 12-well plates with 24-hour incubation, then treated with peptides or SAHA for another 24 or 48 hours. The cells were washed with PBS and harvested using the lysis buffer (50 mmol/L Tris-Cl, PH = 6.8, 2% SDS, 6% glycerol, 1% β-mercapitalethanol, 0.004% bromophenol blue). The extracted protein concentrations were measured by a spectrophotometer (Nano-Drop ND-2000). An equal amount of protein was loaded onto a SDS-PAGE gel and resolved by electrophoresis. Protein bands were then transferred to Nitrocellulose Blotting membranes followed by incubation with an appropriate primary antibody overnight at 4°C. Antibody dilutions were used as follows: 1:500 for rabbit monoclonal anti-HDAC1 (Abcam), rabbit monoclonal anti-HDAC6 (Proteintech), rabbit monoclonal anti-H4K16ac (Millipore), and mouse monoclonal anti–Ac-tubulin (Proteintech) and 1:1,000 for rabbit polyclonal anti-H3 (Proteintech), rabbit monoclonal anti-H3K56ac (Millipore), and mouse monoclonal anti-GAPDH (Proteintech). Then, the membranes were washed with buffer (1× TBS, 0.05% Tween 20). Secondary antibodies of goat anti-rabbit or anti-mouse were used for 1-hour incubation at room temperature. Proteins were then visualized with chemiluminescent substrates.

RNA isolation and quantitative RT-PCR

Cells were pretreated as indicated in the Western blot experiment before the RT-PCR experiment. Forty-eight hours after incubation with peptides and SAHA, total RNA was extracted from PA-1 or NTERA-2 cells using TRIzol reagent (Invitrogen) according to the manufacturer's protocol. The isolated mRNA was quantified by a spectrophotometer (Nano-Drop ND-2000). Total RNA (2 μg) was reverse transcribed to cDNA using the reverse transcriptase kit (Takara) according to the manufacturer's instructions. The mRNA levels of the target genes were detected by real-time PCR using SYBR green (Takara) in an ABI Prism 7500 real-time PCR system (Applied Biosystems). Data represent two independent experiments with three technical replicates per experiment. Relative changes in transcript levels for each sample were determined by normalizing to β-actin housekeeping gene mRNA levels. Primers were shown in Supplementary Table S1.

Flow cytometry analysis

Transfection efficiency. To detect cell permeability by flow cytometry, all cells were incubated with 10 μmol/L FITC-labeled peptides for 4 hours in medium with 5% FBS at 37°C. After washing with media, the cells were harvested by trypsinization and washed twice with PBS. To quench extracellular fluorescence, the cells were incubated with 0.05% trypan blue for 3 minutes prior to fluorescence activated cell sorting (FACS) analysis.

Apoptosis assay. The apoptosis assay was performed according to the manufacturer's instructions using an Annexin V: FITC Apoptosis Detection Kit I (BD Pharmingen). Briefly, PA-1 cells were seeded in a 12-well plate and allowed to grow for 24 hours in medium with 10% FBS. Then, the cells were treated with different peptides in medium with 5% FBS for 24-hour incubation. The cells were harvested by trypsinization and washed twice with PBS and suspended in 1 × binding buffer. The suspended cells were treated with FITC-labeled Annexin V and propidium iodide (PI) as the protocol indicated. The suspended cells were stained with PI and Annexin V and then analyzed by flow cytometry to determine apoptotic cells. Cells with positive fluorescence intensity signals for both FITC and PI were used for apoptotic cell count.

Cell-cycle analysis. As for the cell-cycle arrest experiments, PA-1 cells were seeded in a 12-well plate and allowed to grow for 24 hours in medium with 10% FBS. The cells were treated with 20 μmol/L peptides in medium of 5% FBS for 24-hour incubation. Then, the cells were washed twice with PBS and harvested by trypsinization. The cells were fixed with cold 70% ethanol for

Downloaded from cancerres.aacrjournals.org on August 7, 2019. © 2019 American Association for Cancer Research.

Published OnlineFirst March 6, 2019; DOI: 10.1158/0008-5472.CAN-18-1421

4 hours and isolated by centrifugation at 2,000 rpm for 5 minutes. Then, the precipitant cells were suspended in PBS with 1% Triton-100, 5 mg/mL PI, 1 mg/mL RNase and stained at 37°C for 30 minutes. The samples were detected by flow cytometer and the percentages of cells in G_0–G_1, S, and G_2–M phases were analyzed by FlowJo software.

Confocal microscopy

PA-1 cells (or other cancer cells) were seeded in 24-well culture plate on coverslips. The cells were grown in DMEM with 10% FBS (v/v) in a 37°C, 5% CO_2 incubator for 24 hours. The cells were incubated with 10 μmol/L peptides for 4 hours at 37°C. Then, the cells were washed 3 times with PBS and then fixed with 4% (wt/vol) formaldehyde (Alfa Aesar, MA) in PBS for 30 minutes. They were then washed 3 times with PBS and stained with 6-diamidino-2-phenylindole (DAPI; Invitrogen) for 10 minutes. Images of peptide localization in cells were taken via confocal laser scanning microscope (FV1000, Olympus). Image processing was done using the Volocity software package (Zeiss Imaging).

Lactate dehydrogenase release

The lactate dehydrogenase (LDH) release assay was used to detect the cell membrane damage and performed by the LDH release kit (Dojindo). PA-1 cells were seeded in a 96-well plate at a density of 5×10^3 cells/well. Then, the cells were treated with 100 μL peptides with 2-fold serial dilution starting at 80 μmol/L for 12 hours at 37°C. Lysis buffer was added as positive control and incubated at 37°C for 30 minutes. Then, 100 μL working solution was added to each well and incubated for 30 minutes at room temperature. The reaction was stopped by 50 μL stop solutions and detected immediately at 490 nm absorption by a microplate reader (PerkinElmer, Envision). LDH release activity was calculated by [(ODsamples − ODblank)/(ODpositive − ODblank)] × 100.

Hemolysis assays

Fresh mouse red blood cells were collected and centrifuged at 1,500 rpm for 10 minutes. Erythrocytes were washed 4 times and then resuspended in 0.9% NaCl to a final density of 10^8/mL. A serial dilution of peptides was added staring at 200 μmol/L and incubated at 37°C for 1.5 hours. Then, rythrocytes were centrifuged at 6,000 rpm for 10 minutes and the release of hemoglobin was monitored by measuring the absorbance of supernatant at 570 nm by a microplate reader (PerkinElmer, Envision). Triton X-100 (0.1%) and 0.9% NaCl were used as positive and negative controls, respectively. The percentage of hemolysis was calculated according to the following equation: %Hemolysis = [($A_{576\ nm}$ of sample − $A_{576\ nm}$ of negative control)/($A_{576\ nm}$ of positive control − $A_{576\ nm}$ of negative control)] × 100.

Streptavidin pulldown assay

PA-1 cells were maintained in MEM containing 10% FBS and penicillin/streptomycin for 24 hours. Whole-cell extracts were generated using lysis buffer [50 mmol/L Tris (pH 8.0), 150 mmol/L NaCl, 1 mmol/L EDTA, 0.5% Nonidet P-40]. Protein concentration of the soluble fraction was measured by a spectrophotometer (Nano-Drop ND-2000). Biotinylated peptides (40 μmol/L) were added to protein extracts (500 μg) and incubated at 4°C overnight. Then, the mixture was incubated with Streptavidin Magnetic Beads (Thermo) at room temperature for 2 hours. The beads were collected and washed 3 times with lysis buffer, eluted by boiling in SDS buffer, and subjected to Western analysis with HDAC antibody.

Immunoprecipitation

Exponentially growing PA-1 cells (10 cm dish) were treated with 10 μmol/L peptide 16cyc-HxA or equivalent volume of DMSO for 16 hours. Whole-cell extracts were generated using lysis buffer [50 mmol/L Tris (pH 8.0), 150 mmol/L NaCl, 1 mmol/L EDTA, 0.5% Nonidet P-40]. Protein extracts (500 μg) were precleared for 1 hour with 40 μL protein A sepharose beads (50%, Sigma) before the addition of the indicated antibodies. Then, pretreated cell extracts were incubated with 2 μg rabbit antibody anti-HDAC1(Abcam) or anti-LSD1(Abcam) overnight at 4°C. The mixture was incubated with protein A sepharose beads at 4°C for 2 hours. The beads were washed five times with cold lysis buffer. Precipitated proteins were subjected to Western blotting analysis.

Chromatin immunoprecipitation assays

For chromatin immunoprecipitation (ChIP) assays, 1×10^7 to 5×10^7 PA-1 cells were used for each sample. Proteins were crosslinked to DNA by addition of formaldehyde to a final concentration of 1.0% for 10 minutes at room temperature. After incubating with 125 mmol/L glycine for 5 minutes, cells were harvested using cold PBS and resuspended in FA lysis buffer (50 mmol/L HEPES-K^+, pH 7.5, 140 mmol/L NaCl, 1 mmol/L EDTA pH 8.0, 1% Triton X-100, 0.1% sodium deoxycholate, 0.1% SDS, protease inhibitors), and sonicated to generate DNA fragments of 500 to 1,000 bp in average length. Soluble chromatin fragments were incubated with 2 μg primary antibodies or IgG overnight. Immunocomplexes were incubated with protein A sepharose beads for 2 hours, briefly centrifuged, and washed sequentially with the wash buffer (0.1% SDS, 1% Triton X-100, 2 mmol/L EDTA, 150 mmol/L NaCl, 20 mmol/L Tris-HCl, pH 8.0) three times and the final wash buffer (0.1% SDS, 1% Triton X-100, 2 mmol/L EDTA, pH 8.0, 500 mmol/L NaCl, 20 mmol/L Tris-HCl, pH 8.0) one time. Immunocomplexes were eluted, and the crosslinks were reversed in the elution buffer (1% SDS, 0.1 mol/L NaHCO3) at 65°C. Purified DNA was quantified by real-time qPCR. Sequences of the primers used for ChIP assays are listed in Supplementary Table S2.

In vivo antitumor efficacy of peptides in a mouse tumor xenograft model

Athymic nude mice (BALB/c ASlac-nu) were obtained from Vital River Laboratory Animal Technology Co. Ltd. of Beijing, People's Republic of China and allowed an acclimation period of 1 week. Mice were maintained in an isolated biosafety facility for specific pathogen-free animals with bedding, food, and water. All operations were carried out in accordance with the National Standard of Animal Care and Use Procedures at the Laboratory Animal Center of Shenzhen University, Guangdong Province, People's Republic of China (the permit number is SZU-HC-2014-02).

For tumor suppression assay, we first harvested PA-1 cells or NTERA-2 cells and resuspended in DMEM at a density of 1×10^8/mL. Then, athymic nude mice (female; 6 weeks old) were inoculated with 1×10^7 PA-1 cells or NTERA-2 cells (100 μL volume of each) propagated *in vitro* subcutaneously in the lower flank of mice. After 15–20 days, mice with tumors

Downloaded from cancerres.aacrjournals.org on August 7, 2019. © 2019 American Association for Cancer Research.

Published OnlineFirst March 6, 2019; DOI: 10.1158/0008-5472.CAN-18-1421

exceeding 100–200 mm^3 in volume were randomly divided into 5 groups of 5–6 mice per treatment group. Mice bearing PA-1 or NTERA-2 tumors were intraperitoneally injected with peptides (50 mg/kg) or SAHA (50 mg/kg) using PBS as a negative control. Mice were injected every other day starting on day 0. Tumor volumes were measured by calipers (accuracy of 0.02 mm) every other day and calculated using the following formula: $V = L \times W^2/2$ (W being the shortest dimension and L the longest dimension). Each tumor was independently measured and calculated by changes in volume (folds) relative to day 0. Statistical significances between groups were tested by one-way analysis of variance.

In vivo imaging

When the tumor reached an appropriate volume of 100–200 mm^3, mice were injected with Cy5-labeled 16cyc-HxA and 16lin-HxA peptides by intratumoral injection at 50 mg/kg. After injection, mice were anesthetized with 100 μL 1% pentobarbital sodium. Once the mice were properly anesthetized, they were imaged at indicated time points to monitor the accumulation of cyc5-labeled peptides in tumors using the CRI Maestro ex/in vivo imaging system (ex: 605 nm; filter: 700 nm).

Preparation of paraffin section histologic analysis

The mice were sacrificed after 21 days treatment, and organ and tumor tissues were collected and fixed in 4% buffered formalin-saline at room temperature for 24 hours for histologic experiments. Then, the tissues were embedded in paraffin blocks, and paraffin sections of 4-mm thickness were mounted on a glass slide for hematoxylin and eosin (H&E) staining. The H&E staining slices were examined under a light microscopy (Olympus BX51). For IHC assay, the ovarian cancer tissue microarray slides were immersed in 3% H_2O_2 for 5 minutes to inactivate the endogenous peroxidase. BSA (5%) was used to block the nonspecific binding sites for 15 minutes. Antibodies against HDAC1, HDAC6, H3K56ac, H4K16ac, and caspase-3 were diluted as the primary antibodies and incubated with slides at 4°C overnight. The samples were washed and then incubated with Rabbit-Probe or Mouse-Probe MACH3 HRP-polymer detection system according to the supplier's instructions. Slides were developed with 3,3′-diaminobenzidine substrate using the ImmPACT DAB Peroxidase Substrate Kit (Vector Laboratories) for 1–5 minutes, counterstained with hematoxylin. (All reagents were obtained from Biocare Medical.)

Mice voluntary cage-wheel exercise

BALB/c mice (female; 6 weeks old) were obtained from Vital River Laboratory Animal Technology Co. Ltd. of Beijing, People's Republic of China and allowed an acclimation period of 1 week at 22 ± 2°C with a 12-hour light–dark cycle (lights on 8 am, lights off 8 pm). Subsequently, BALB/c mice were randomly divided into 5 groups (4–5 mice per group) and were subcutaneously treated with PBS, peptides or SAHA (50 mg/kg), respectively, via intraperitoneal injection every other day. A voluntary running system consisting of six separated chambers (Chengdu TME Technology Co., Ltd) was used in the animal performance study. During the training session, mice were placed on the motorized rod (30 mm in diameter) in the chamber. Rotation speed gradually increased from 0 to 100 rpm over the course of 100s. The rotation speed was recorded when the animal fell off from the rod. Performance was measured as the average rotation speed animals achieved during the training session. The different groups were all trained in five same continuous time points (days 0, 2, 4, 8, 10, 12, 14, 16, 18, and 20). No significant differences were found between these five groups.

Results

Design and enzymatic analysis of peptide-based HDAC inhibitors

In 2016, Watson and colleagues developed a substrate-like peptide inhibitor based on the HDAC1-specific substrate H4K16, with K16 replaced with a hydroxamic acid functionality, which showed nanomolar HDAC1 inhibition (27). The crystal structure of the HDAC1–MTA1 complex with this peptide revealed that the peptide alone can make complementary contact with the rim of the HDAC active site. This is a new attempt to develop a substrate mimic for HDAC inhibition. However, calls for further study on the cellular functions of this peptide inhibitor remain unanswered. Herein, we chose to mimic another HDAC1-specific substrate, H3K56, based on the preferential deacetylation of HDAC1 on H3K56. The crystal structure of H3 indicates that H3K56 is on the C terminus of the α-helical region of H3 (comprising residues 45–56), suitable for incorporation of hydroxamic acid at K56 and N-terminal stabilization using the TD strategy (23, 28). Thus, we chose to modify the helical region (comprising residues 45–56), and a detailed design is shown in Fig. 1A and Supplementary Table S3. The three additional arginines on the N-terminus of peptides were used to enhance their cellular penetration. To study the structure and activity relationship, enzyme inhibition assays were performed on peptides with different lengths or sequences toward HDACs from HeLa nuclear extract shown in Fig. 1B (HeLa nuclear extract is reported to mainly contain HDAC1/2 protein, which was validated in Supplementary Fig. S1A and S1B; refs. 29–31). The peptide 16cyc-HxA showed better HDAC1/2 enzyme inhibition, emphasizing the importance of proper peptide sequences (Fig. 1B). Similar to TSA, the peptides 16cyc-HxA showed pan-HDAC inhibition shown in Fig. 1C, but minimal effect on the NAD^+-dependent SIRT1 enzyme (Supplementary Fig. S2A and S2B). The pan-HDAC inhibition may be due to the high homology of enzyme pocket in HDAC isoforms including HDAC1, which can tightly bind to hydroximic acid. Although HDAC1 preferably binds to H3K56, the strong binding of hydroximic acid and the flexibility of peptide H3K56 still somehow rendered bindings with other isoforms. The 16cyc-HxA was more potent than 16lin-HxA, suggesting that helical stabilization can enhance target-binding affinity (Supplementary Figs. S3A–S3B and S4A–S4D). Despite their limited HDAC isoform selectivity, we believe with further understanding of the interactions between HDACs with their partners, isoform-selective HDAC inhibitors will emerge through precise adjustment of peptide structure.

Cellular permeability and antiproliferation of peptide inhibitors in various cell lines

To better investigate the cellular functions of these peptide inhibitors in different cell lines, cellular uptake efficiency and intracellular distribution were tested by cell flow cytometry and confocal microscopy shown in Fig. 2A and B and Supplementary Figs. S5A–S5B to and S8A–S8B. FITC-labeled TAT is a commonly used cell-penetrating peptide derived from HIV integrase (32). The cyclic peptide 16cyc-HxA showed better

Downloaded from cancerres.aacrjournals.org on August 7, 2019. © 2019 American Association for Cancer Research.

Published OnlineFirst March 6, 2019; DOI: 10.1158/0008-5472.CAN-18-1421

A

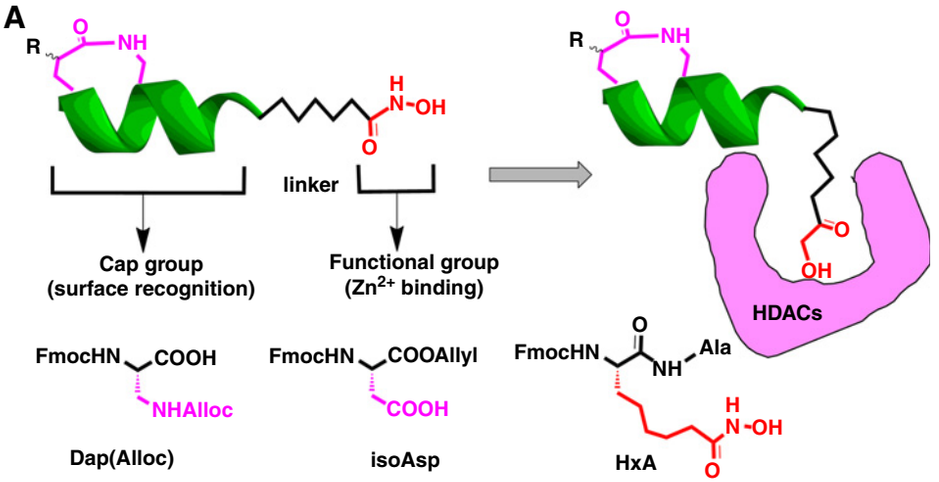

B

Summary of peptide inhibitors toward HeLa nuclear extract (mainly HDAC1/2)

Peptide	Sequence	IC_{50} (nmol/L) (HeLa nuclear extract)
4lin-HxA	Ac-YQHxA	928 ± 83
9lin-HxA	Ac-REIRRYQHxA	226 ± 10
13lin-HxA	Ac-TVALREIRRYQHxA	217 ± 2
16lin-HxA	Ac-RRR-TVALREIRRYQHxA	255 ± 51
13cyc-HxA	Ac-isoAspVADapREIRRYQHxA	256 ± 41
16cyc-HxA	Ac-RRR-iso-AspVADapREIRRYQHxA	151 ± 6
16KA	Ac-RRR-iso-AspVADapREIRRYQKA	>10,000
Scr-1	Ac-RRR-iso-AspRRDapREVAIYQHxA	320 ± 17
Scr-2	Ac-IEY-iso-AspVADapQRRRRRRHxA	496 ± 68
TSA	Positive control	19.51 ± 5.6

HeLa nuclear extract = 0.2 mg/mL, substrate = 100 μmol/L Boc-Lys(Ac)-AMC, the assays were performed according to HDAC Activity Fluorometric Assay Kit (from BioVision). Error bars represent SEMs of at least three independent measurements.

C

Summary of peptide inhibitors toward different HDAC isoforms

Peptide	IC_{50}/nmol/L			
	HDAC1	HDAC3	HDAC6	HDAC8
16cyc-HxA	303 ± 74	121 ± 3	99 ± 20	133 ± 4
16lin-HxA	777 ± 164	503 ± 33	180 ± 25	592 ± 29
16KA	>10,000	>10,000	>10,000	>10,000
TSA	161.3 ± 15	92.7 ± 0.3	44.9 ± 4	61.8 ± 3

All assays above were performed according to the assay kit: HDAC1 Inhibitor Screening Assay Kit from Cayman Chemical; HDAC3, HDAC6, HDAC8 Inhibitor Screening Assay Kit from Biovision. Error bars represent SEMs of at least three independent measurements.

Figure 1.
The enzymologic analysis of our designed peptide inhibitors. **A,** The design of peptide-based HDAC inhibitors. **B,** Summary of peptide inhibitors toward HeLa nuclear extract (mainly HDAC1/2). **C,** Summary of peptide inhibitors toward different HDAC isoforms. Detailed information about enzyme activity assays is also shown in **B** and **C**.

Downloaded from cancerres.aacrjournals.org on August 7, 2019. © 2019 American Association for Cancer Research.

Published OnlineFirst March 6, 2019; DOI: 10.1158/0008-5472.CAN-18-1421

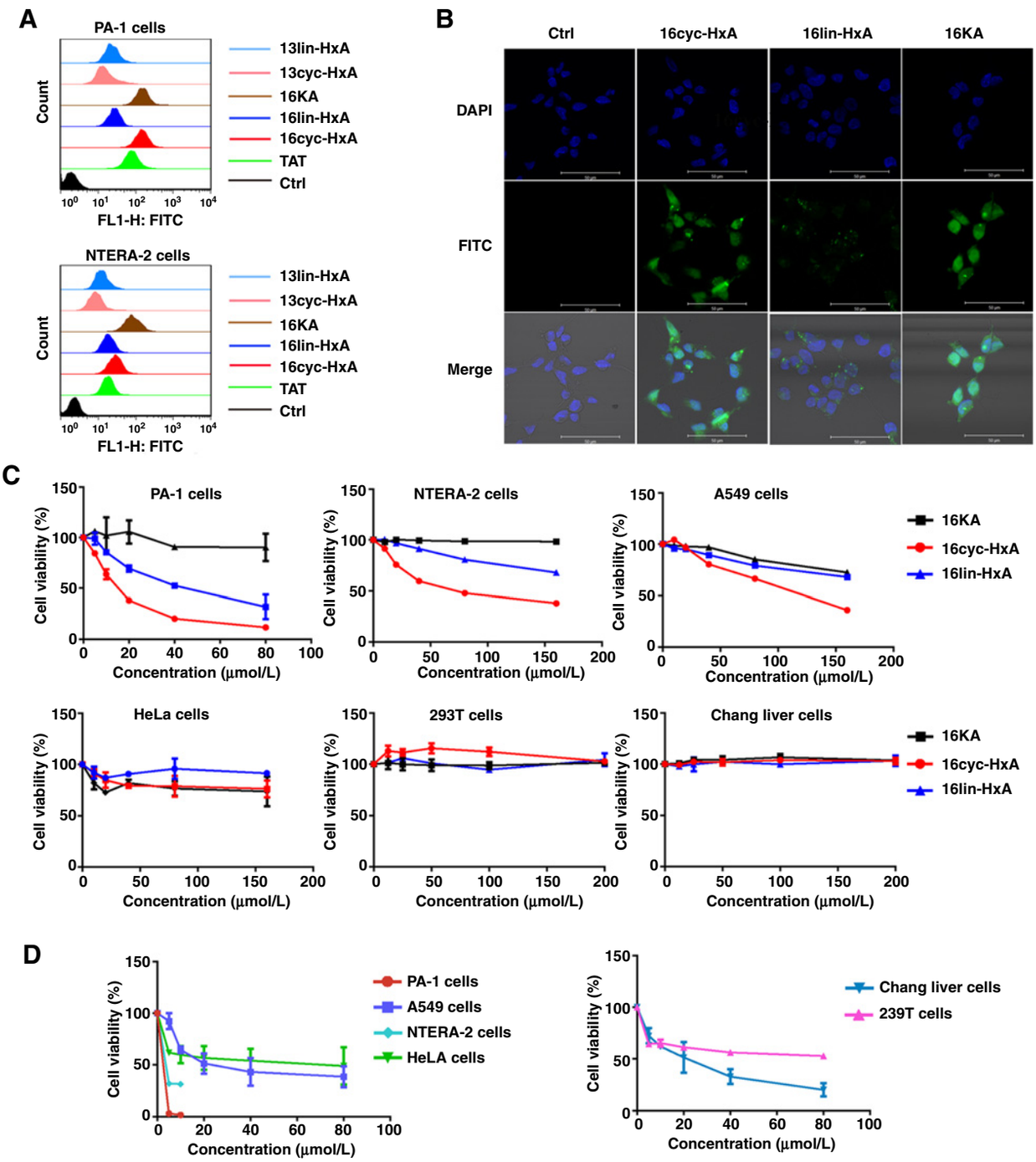

Figure 2.

Cellular permeability and antiproliferation effect in different cell lines treated with peptide inhibitors. **A,** Representative histogram plot from flow cytometry analysis in the PA-1 and NTETA-2 cell lines, where the *y*-axis represents cell counts and the *x*-axis represents FITC fluorescence intensities. PA-1 cells or NTERA-2 cells were treated with 10 μmol/L FITC-labeled peptides for 4 hours and analyzed after incubation with 0.05% trypan blue for 3 minutes. **B,** Confocal microscopy images obtained in PA-1 cells. Scale bar, 50 μm. **C,** Viability of PA-1, NTERA-2, A549, HeLa, HEK-293, and Chang liver cells. PA-1 cells were incubated with 5, 10, 20, 40, and 80 μmol/L peptides for 48 hours; other cell lines were incubated with 10, 20, 40, 80, 160 μmol/L peptides for 48 hours. **D,** Viability of different cell lines treated with positive control SAHA. PA-1 and NTERA-2 cells were incubated with 0.625, 1.25, 2.5, 5, and 10 μmol/L SAHA for 48 hours; other cell lines were incubated with 5, 10, 20, 40, and 80 μmol/L SAHA for 48 hours. Error bars represent SEMs of at least three independent measurements.

Downloaded from cancerres.aacrjournals.org on August 7, 2019. © 2019 American Association for Cancer Research.

Published OnlineFirst March 6, 2019; DOI: 10.1158/0008-5472.CAN-18-1421

cellular uptake than the other tested peptides. In addition, all of the peptides had better cell-penetrating ability in PA-1 cells over any of the other cell lines. The mechanisms of peptide cellular uptake are a focused research area but still far from been fully elucidated (33). Synergetic contribution from peptides' secondary structure, amphiphilicity, and charges correlates with peptides' cellular uptake (34). Different types of cells with different membrane compositions and different expressed receptors made the question more elusive. Intracellular fluorescence at different periods of time indicated the peptide 16cyc-HxA had good cellular stability shown in Supplementary Fig. S9A–S9C.

As cell penetration is a prerequisite for cellular functions, we chose the cell-penetrating peptides 16cyc-HxA, 16lin-HxA, and 16KA to further study their cellular functions. We chose pluripotent human ovarian teratocarcinoma PA-1 cells and testicular embryonic carcinoma NTERA-2 cells as they are well-accepted models for studying cancer cell stemness and are highly sensitive to HDAC1 (15, 35–37). The approved drug SAHA was chosen as a positive control. As shown in Fig. 2C, in cancer stem–like cells, cyclic peptide 16cyc-HxA showed a significant antitumor effect, with an IC_{50} of 14.65 μmol/L in PA-1 cells and an IC_{50} of 62 μmol/L in NTERA-2 cells, better than 16lin-HxA. Notably, peptide 16KA did not have a significant effect on these cells. Compared with the two scrambled peptides Scr-1 and Scr-2, 16cyc-HxA showed better antitumor effects to PA-1 cells; nevertheless, this peptide showed weaker cellular uptake than Scr-2, ruling out the possibility that the peptide's high efficiency was simply caused by increased cellular uptakes as shown in Supplementary Fig. S10A–S10C. In the other two cancer cell lines, A549 cells and HeLa cells, peptide 16cyc-HxA displayed a decreased effect, partly because they were reported to be less sensitive to HDACs (15, 36). The negligible effect on the two normal cell lines indicated the low nonspecific toxicity of these peptides. Notably, SAHA exhibited potent toxicity across all cell lines, including the normal ones (Fig. 2D). To further study the HDAC isoform-related cytotoxicity, the class I selective small inhibitors MS275 and HDAC6 and selective small inhibitors Tubacin were selected as positive controls shown in Supplementary Fig. S11A–S11C. In PA-1 and NTERA-2 cells, both SAHA and MS275 had potent antitumor effect, while Tubacin had much weaker antitumor effects, indicating the importance of class I HDACs in cancer stem–like cells. Meanwhile, these small inhibitors all showed similar toxicity to normal cells. The nonspecific toxicity of these peptide inhibitors was further excluded using the LDH release assay in PA-1 cells (Supplementary Fig. S12A and S12B) and the hemolysis assay (Supplementary Fig. S13A and S13B). In summary, peptide 16cyc-HxA exhibited preferential inhibition on cancer stem–like cells, PA-1 cells or NTERA-2 cells, which was sensitive to HDAC1 inactivation. Importantly, the nonspecific toxicity of peptide inhibitors suggested their superiority based on a wider safety window over SAHA.

Peptide inhibitors inactivate an HDAC signal pathway in cancer stem–like cells

To investigate the association between HDAC inactivation and antiproliferation in cancer stem–like cells, we used an *in vitro* streptavidin pulldown assay to test whether our designed peptides could bind to HDACs endogenously expressed in PA-1 cells (Fig. 3A; Supplementary Fig. S14A). We first tested the expression levels of these HDAC isoforms in PA-1 cells as shown in Supplementary Fig. S14A. HDAC1 showed much higher expression than other isoforms. Streptavidin pulldown assays indicated that peptide 16cyc-HxA and 16lin-HxA could bind to class I HDACs (HDAC1, -2, -3, -8) and class II HDACs (HDAC4, -5, -6), but minimal binding to class III (SIRT 1 and SIRT 6) shown in Supplementary Fig. S14B, which was also supported by SIRT1 inhibition experiments shown in Supplementary Fig. S2A and S2B. The trapping of HDAC1 and HDAC6 depended on the concentration of the peptides shown in Supplementary Fig. S14C and S14D.

We subsequently detected representative acetylation changes of HDAC1-specific substrates (H3K56 and H4K16) and an HDAC6-specific substrate (α-tubulin) in PA-1, NTERA-2, and A549 cells (Fig. 3B; Supplementary Fig. S15A and S15B). In these cell lines, peptides 16cyc-HxA and 16lin-HxA significantly increased the acetylation of H3K56, H4K16, and α-tubulin in a dose-dependent way, indicating the cellular inactivation of HDAC1 and HDAC6 without downregulating their expression indicated in Supplementary Fig. S15A and S15B. Meanwhile, peptides 16cyc-HxA and 16lin-HxA showed irreversible HDAC inhibition in PA-1 cells for 48-hour treatment (Supplementary Fig. S16A and S16B). The positive controls SAHA and MS275 showed more obvious effect on the acetylation of H3K56 and H4K16, and Tubacin showed preference for the acetylation of tubulin shown in Supplementary Fig. S17A and S17B, which further suggested the inactivation of HDAC1 and HDAC6 of 16cyc-HxA.

Most of HDACs performed their distinct functions by forming multiple protein complexes, among which, CoREST complex containing HDAC1, LSD1, and CoREST are reported to play a key role in cancer stem–like cells and have attracted special interests (15, 38). In this study, we found that 16cyc-HxA could upregulate the expression of P21 and P53, significantly stimulate mono- and dimethylation of H3K4 in PA-1 cells, suggesting the inactivation of LSD1 (Fig. 3C; Supplementary Fig. S18). To further study the peptide influence on the LSD1-CoREST-HDAC1 complex, CO-IP assays were performed and demonstrated that peptide 16cyc-HxA could disrupt their interactions as shown in Fig. 3D. Meanwhile, the peptide inhibitors could alter the recruitment of HDAC1 or LSD1 to Sox2 promoters by the ChIP experiment shown in Supplementary Fig. S19A and S19B. We also found that inactivation of HDACs could downregulate the expression of the pluripotent stem cell marker Sox2 (Fig. 3C and E), verifying that HDAC inactivation could induce cell differentiation of cancer stem–like cells.

Loss of HDACs can cause cell differentiation and induce the expression of genes associated with cell cycle, such as *P21* (39). Significant downregulation of the stemness gene *Sox2* and upregulation of the differentiation gene *FoxA2* are convincing evidence of CSC differentiation (15). To further investigate whether our designed peptides could influence related gene expression, we monitored the expression of the genes *Sox2*, *FoxA2*, and *P21* by quantitative RT-PCR (Fig. 3E). Compared with SAHA and 16lin-HxA, peptide 16cyc-HxA could significantly activate the expression of the *FoxA2* and *P21* genes and downregulate the expression of the *Sox2* gene in both PA-1 cells and NTERA-2 cells. Together, these data indicated that deactivation of HDACs by our designed peptides could interrupt the LSD1-CoREST-HDAC1 complex and might induce the cancer stem–like cells to differentiation.

Downloaded from cancerres.aacrjournals.org on August 7, 2019. © 2019 American Association for Cancer Research.

Published OnlineFirst March 6, 2019; DOI: 10.1158/0008-5472.CAN-18-1421

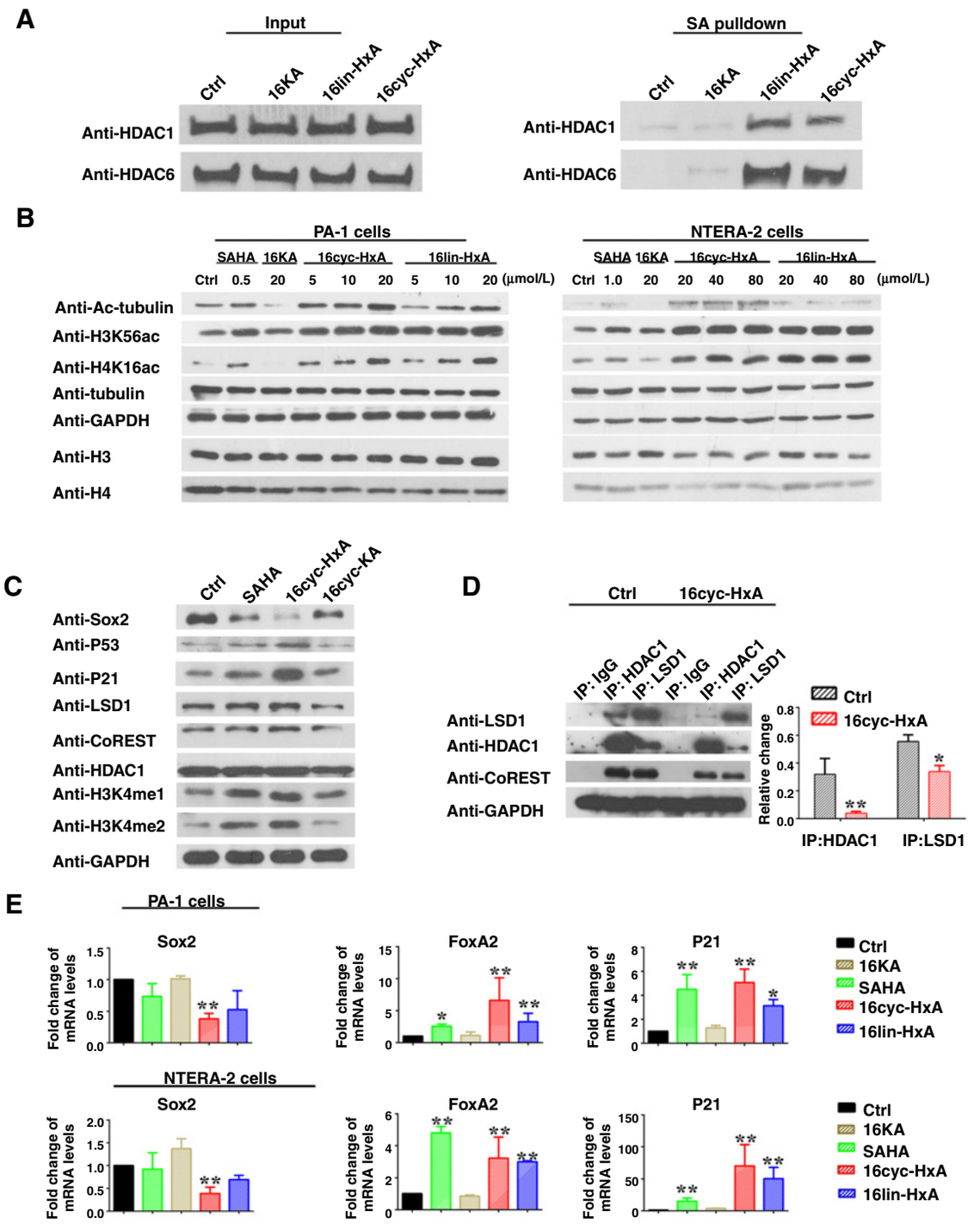

Figure 3.

The inactivation of HDACs in cancer stem–like cells (PA-1 and NTERA-2 cells). **A,** Cellular binding affinity of peptide inhibitors (40 μmol/L) to HDAC1 and HDAC6 in PA-1 cell lysates. **B,** The acetylation level of HDAC substrates in PA-1 cells and NTERA-2 cells treated with peptides and SAHA in different concentration, PA-1 cells for 24 hours, and NTERA-2 cells for 48 hours. **C,** HDAC-related protein expression in PA-1 cells incubated with 20 μmol/L peptides or 0.5 μmol/L SAHA for 24 hours. **D,** The peptide 16cyc-HxA disrupted the interaction between LSD1-CoREST-HDAC1 complex in PA-1 cells. The cells were treated with 10 μmol/L peptide inhibitors for 16 hours. The results were further analyzed using Gel-Pro Analyzer. IP: HDAC1, the ratio of anti-LSD1/anti HDAC1/GAPDH from control or 16cyc-HxA with the same sample. IP: LSD1, the ratio of anti-HDAC1/anti-LSD1/GAPDH from control or 16cyc-HxA with the same sample. **E,** The mRNA levels of HDAC-related genes *Sox2, FoxA2*, and *P21* in PA-1 cells or NTERA-2 cells incubated with 20 μmol/L peptides or 1 μmol/L SAHA for 48 hours. Fold changes of mRNA levels were analyzed by quantitative PCR. Error bars represent SEMs of at least three independent measurements. *, $P < 0.05$; **, $P < 0.01$ versus control. SA, streptavidin.

Downloaded from cancerres.aacrjournals.org on August 7, 2019. © 2019 American Association for Cancer Research.

Published OnlineFirst March 6, 2019; DOI: 10.1158/0008-5472.CAN-18-1421

Inactivation of HDACs induced cell apoptosis and cell-cycle arrest in cancer stem–like cells

The aberrance of HDACs is reported to be associated with cellular functions such as cell apoptosis and cell-cycle arrest (40). To verify if our designed peptides could induce cell apoptosis, Annexin V/PI assay was performed as shown in Fig. 4A and Supplementary Fig. S20A and S20B. The peptide 16cyc-HxA had greater apoptotic effect than 16lin-HxA in PA-1 and NTERA-2 cells. To investigate whether the apoptotic effect was mediated by a caspase-3-dependent pathway, PA-1 cells or NTERA-2 cells were treated with peptide inhibitors and finally analyzed using a caspase-3 assay kit (Fig. 4B) or Western blot assays (Supplementary Fig. S21). The activation of caspase-3 demonstrated that peptide inhibitors could induce the caspase-3-dependent apoptosis pathway.

HDAC inhibition has been shown to have antiproliferative effects through the induction of cell-cycle arrest in G_1 or G_2 (40). To study the alteration of cell-cycle distribution of our designed peptides, FACS assays were performed as shown in Fig. 4C and Supplementary Fig. S22. The peptide 16cyc-HxA displayed a more appreciable arrest of cell-cycle progression in G_2–M phase than peptide 16lin-HxA. The 16KA-treated group

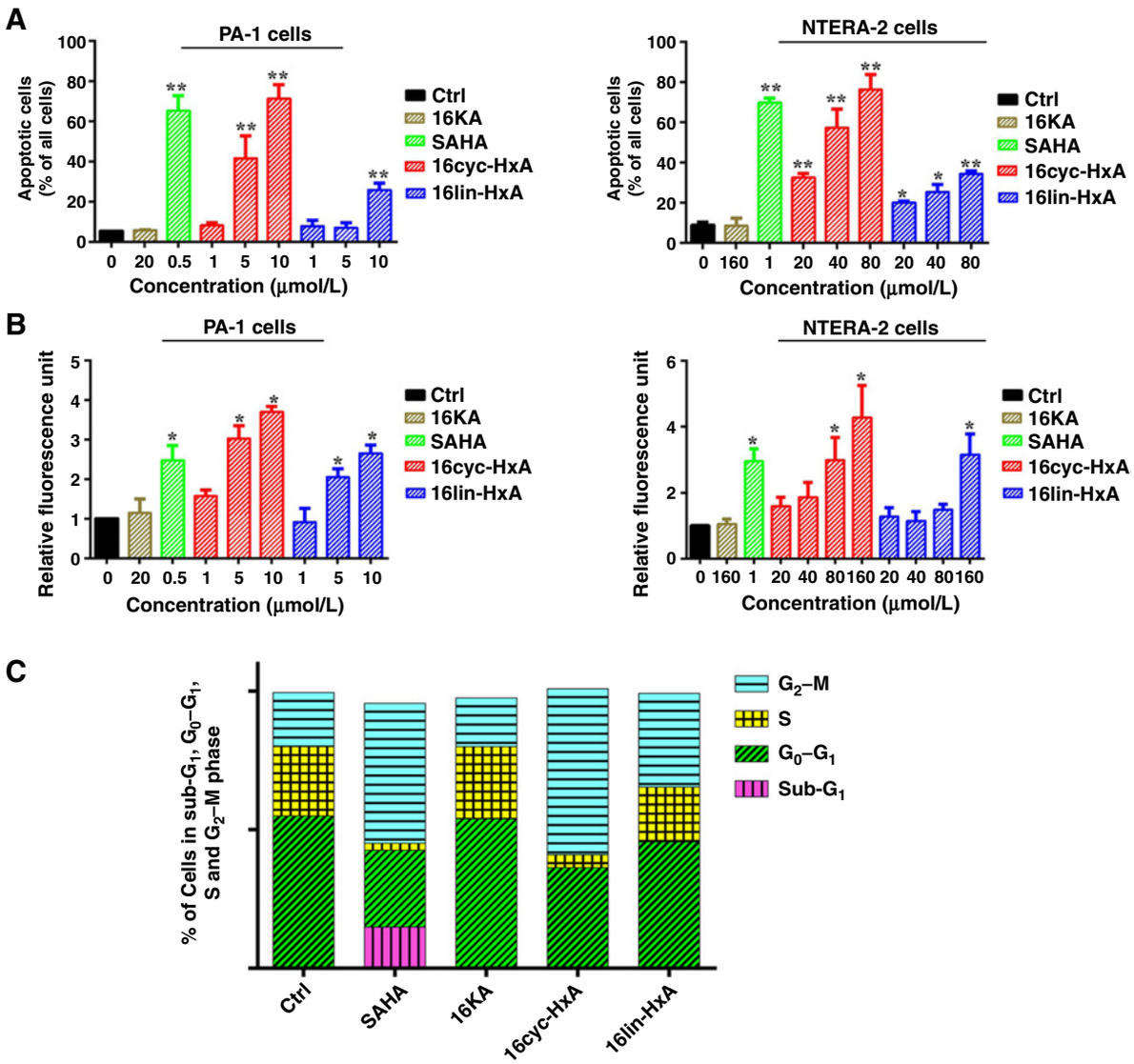

Figure 4.

Inactivation of HDACs can cause cell apoptosis and cell-cycle arrest. **A,** The number of apoptotic cells stained with FITC–Annexin V/PI was measured by flow cytometry. PA-1 cells were treated with peptide inhibitors or SAHA for 24 hours, NTERA-2 cells were treated with peptide inhibitors or SAHA for 48 hours. **B,** Caspase-3 activity was measured by exposing the cells to a caspase-3–specific substrate. PA-1 cells were treated with peptide inhibitors for 24 hours and NTERA-2 cells were treated with peptide inhibitors for 48 hours. Error bars represent SEMs of at least three independent measurements. *, $P < 0.05$; **, $P < 0.01$ versus control. **C,** Cell-cycle distribution of flow cytometry analysis treated with different peptides at 20 μmol/L or SAHA at 0.5 μmol/L for 24 hours in PA-1 cells.

Downloaded from cancerres.aacrjournals.org on August 7, 2019. © 2019 American Association for Cancer Research.

Published OnlineFirst March 6, 2019; DOI: 10.1158/0008-5472.CAN-18-1421

did not show obvious cell-cycle arrest compared with the control group. The cell-cycle results were further confirmed by Western blot assays against cell-cycle marker cyclin A, cyclin B1, P21, and H3PS10 shown in Supplementary Fig. S23A and S23B. Our designed peptides could upregulate the expression of P21, cyclin B1, and H3PS10, but had little effect on the expression of cyclin A, which validated the G_2–M cell-cycle arrest (41, 42).

Transcriptome analysis of the role of HDACs in the proliferation of PA-1 cells

To attain an overview of the genes directly affected by the inactivation of HDACs, genome-wide mRNA microarrays were performed, as shown in Fig. 5 and Supplementary Figs. S24 and S25A–S25C. Compared with DMSO-treated cells, treatment with 16cyc-HxA yielded detection of a total of 2,255 upregulated and 786 downregulated genes (fold change >2), which affected more genes than treatment with peptide 16lin-HxA or SAHA (Fig. 5A and B). The gene ontology analysis revealed that the affected genes are associated with many important signaling pathways relative to widely concerning diseases, such as metabolic diseases, cancer, immune diseases, neurodegenerative diseases, and so on (Fig. 5C; Supplementary Figs. S24 and S25A–S25C). In addition, there are 330 cancer-related genes affected by HDAC inhibition, such as *CDKN1A*, *CDKN1B*, *DNMT3A*, *EGFR*, *NFKB1*, *NFKBIA*, *PIK3*, *WNT*, *BMP4*, *TP53*, *MAPK10*, *NOTCH4*, and so on (Supplementary Table S4). These results were further confirmed by RT-PCR assays and Western blot assays shown in Supplementary Figs. S26 and S27. In summary, all these results demonstrated that inactivation of HDACs had a broad effect on the expression of most genes at the same time, some of which were associated with tumorigenesis.

Peptide inhibitors showed superior antitumor activities in the PA-1 xenograft animal model

To investigate the potential tumor inhibition effect of peptide inhibitors in the PA-1 and NTERA-2 xenograft animal models, we first assessed peptide biocompatibility using the voluntary cage-wheel exercise assay. Over a period of 21 days following injection, voluntary running cycles increased steadily with no significant differences between these five groups, indicating no obvious effects on the motor learning ability of mice (Supplementary Fig. S28A and S28B). Additionally, the body weight of these five groups was not influenced during the 21-day duration of treatment. These findings revealed that the peptides were well tolerated in mice.

Subsequently, we examined the tumor inhibition of these peptides in the PA-1 and NTERA-2 xenograft animal models in nude mice (Fig. 6A–D; Supplementary Fig. S29A–S29D). Tumor-bearing mice were treated with peptides 16cyc-HxA, 16lin-HxA, 16KA, SAHA, or vehicle (5 mice/group, 50 mg/kg, every other day, intraperitoneal injection) for a duration of 3 weeks. We chose this route of administration as it is a common practice for peptide therapeutics referred to previous reports (25, 43). In the PA-1 and NTERA-2 xenograft animal model, in contrast to the vehicle-treated group, peptide 16cyc-HxA resulted in significant inhibition of tumor, at a rate of over 80% (Fig. 6A–C; Supplementary Fig. S29A–S29D). Although the linear peptide was not as stable as the cyclic peptides in the serum stability assay (Supplementary Fig. S30), it also showed an 80% reduction in tumor volume. This phenomenon could most likely be explained by the high dosage of administration (50 mg/kg). The negligible antitumor effect of 16KA excluded the nonspecific toxicity of peptides. The weaker *in vivo* effect of SAHA may be associated with its poor aqueous solubility and low bioavailability by intraperitoneal injection, which may also be the cause of failure to the clinical treatment of solid tumor (44, 45). These peptide inhibitors were also well tolerated in mice based on data for stable body weight (Fig. 6D) accompanied by the lack of any signs of organ lesions by H&E staining (Supplementary Fig. S31A–S31E). The two animal models of cancer stem–like cells provide strong evidence that our peptide inhibitors had great potential for cancer therapy.

To further investigate the peptide distribution *in vivo*, tumor-bearing mice were intratumoral injected with Cy5-labeled 16cyc-HxA and 16lin-HxA followed by imaging at different time points using an ex/*in vivo* imaging system (Supplementary Fig. S30A–S30G). We chose this route of administration as the peptide inhibitors were not labeled with tumor targeting ligands. The optical signal intensity of the Cy5-labeled 16cyc-HxA did not show any diminishment for 24 hours, while the Cy5-labeled 16lin-HxA displayed decreasing signal intensity after 24-hour treatment, suggesting the cyclic peptide was more stable than the linear peptide for *in vivo* tumor therapy.

To detect *in vivo* HDAC inactivation after the 21-day treatment, mice were sacrificed, and tumors were carefully removed for IHC assay (Supplementary Fig. S32A–S32E). When compared with the SAHA-treated group, peptide inhibitors showed more obvious acetylation levels of H3K56 and H4K16, and higher activation of caspase-3, which is consistent with cellular results. Meanwhile, the tumors from mice treated with the two potent peptide inhibitors displayed less cell density than those of the other groups, further confirming the potent anticancer effect. To further check the proliferative index of these tumor tissues, the Ki-67 staining assay was performed as shown in Supplementary Fig. S33, and the peptides (16cyc-HxA and 16lin-HxA) treated tumor tissue had a lower proliferative index than the PBS-treated group, indicating their potent antitumor effects. In summary, our designed peptides showed superior antitumor activities and good biocompatibility in the PA-1 and NTERA-2 xenograft animal model, which is consistent with the cellular results.

Discussion

Developing HDAC inhibitors to efficiently target cancer stem–like cells in combination with other drugs could have great potential to exterminate cancer (46). Recently, HDAC inhibitors have been shown to enhance the sensitivity of pancreatic ductal adenocarcinoma (PDAC) cells to gemcitabine and have the potential to overcome the tumor relapse (47). These studies demonstrate a place for HDACs as promising targets for cancer resistance and elimination.

In the current study, we have developed a new class of stabilized peptide HDAC inhibitors to reduce the cellular nonspecific toxicity of conventional HDAC inhibitors. The helical stabilization method is facile and improves the stability and cellular uptake of these peptides. Unlike the traditional small HDAC inhibitors, the designed peptides showed preferential inhibition of cancer stem–like cells (PA-1 and NTERA-2 cells) and malignant

Downloaded from cancerres.aacrjournals.org on August 7, 2019. © 2019 American Association for Cancer Research.

Published OnlineFirst March 6, 2019; DOI: 10.1158/0008-5472.CAN-18-1421

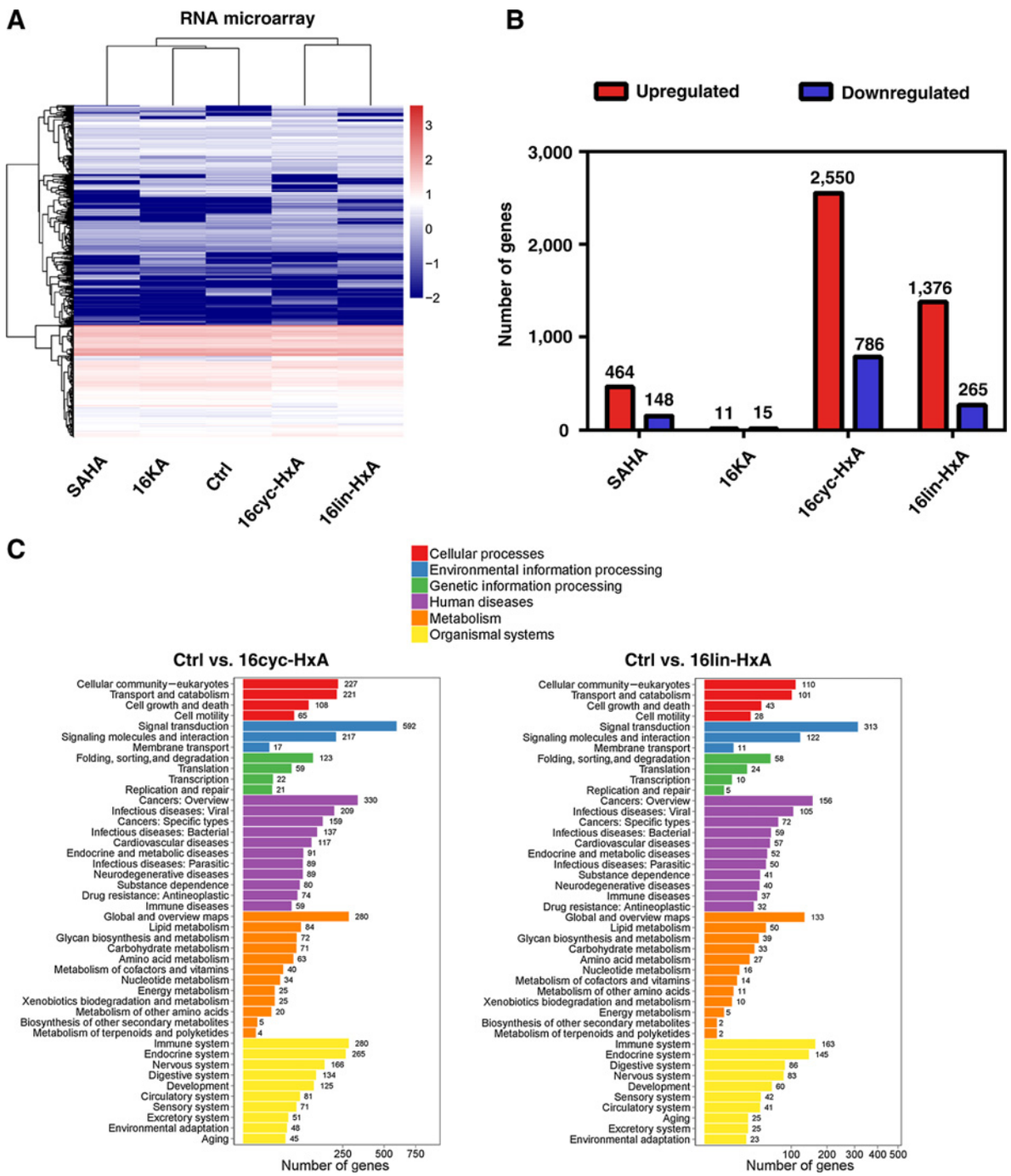

Figure 5.

Transcriptome analysis of PA-1 cells treated with DMSO, 1 μmol/L SAHA, or 20 μmol/L peptides for 48 hours. **A,** RNA-microarray analysis of PA-1 cells treated with SAHA or different peptides compared with DMSO-treated control. **B,** Microarray analysis of upregulated and downregulated genes in PA-1 cells treated with peptides or SAHA. **C,** Gene ontology analysis revealed different signaling pathways influenced by our designed peptides in PA-1 cells.

tumor (A549 cells) cells with negligible effects on normal cell lines (293T and Chang liver cells; Fig. 2). HDACs especially HDAC1 were reported to play an important role in regulating stem cells and cancer stem–like cells, and the inactivation of HDACs could decrease the expression of stemness gene *Sox2*, upregulate differential genes and induce cell death. Although cancer cells and normal cells, such as HeLa cells and 293T cells, were not sensitive to HDAC1 inactivation, peptide inhibitors

Downloaded from cancerres.aacrjournals.org on August 7, 2019. © 2019 American Association for Cancer Research.

Published OnlineFirst March 6, 2019; DOI: 10.1158/0008-5472.CAN-18-1421

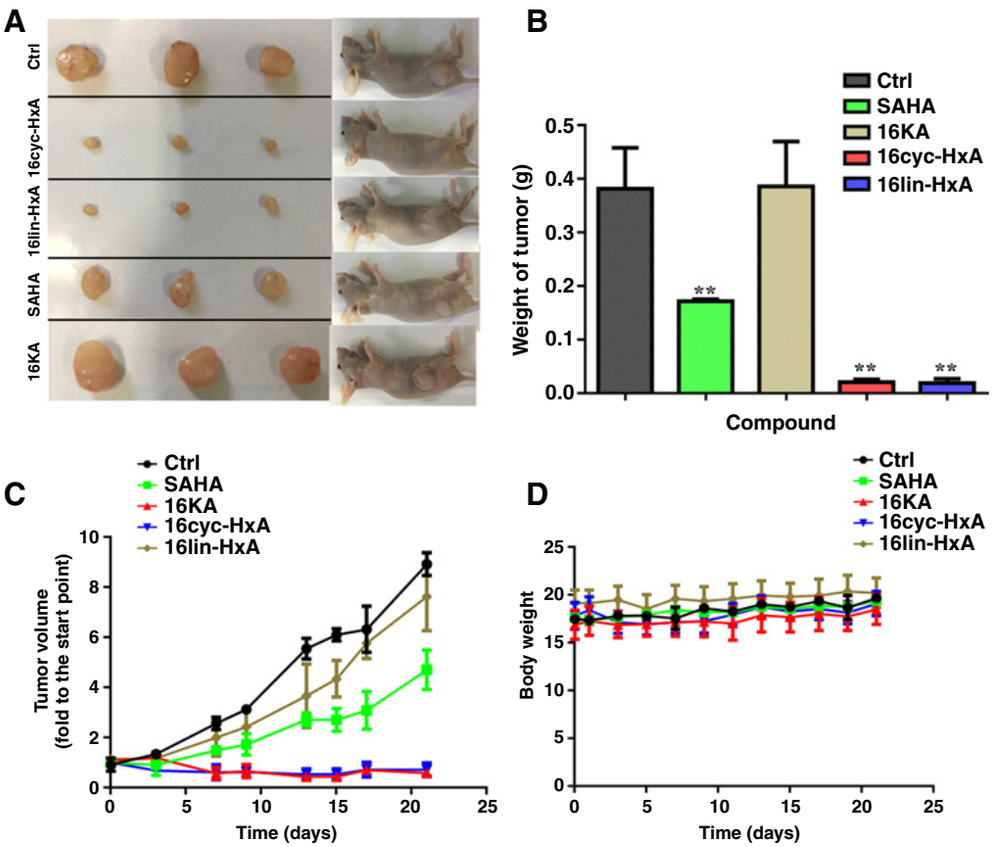

Figure 6.

Antitumor activities of peptides and SAHA in a PA-1 xenograft animal model. **A,** Tumor tissue image of mice treated with PBS (Ctrl), SAHA, peptides 16cyc-HxA, 16lin-HxA, and 16KA at a dosage of 50 mg/kg by intraperitoneal administration. **B,** Tumor weights of mice treated with the same compound as in **A**. **C,** Relative changes of tumor volume over time. **D,** Body weight of mice during the treated time schedule. **, $P < 0.01$ versus ctrl.

showed little toxicity toward HeLa cells. Although peptide 16cyc-HxA showed higher IC_{50} than SAHA itself, it significantly attenuates the nonspecific toxicity of SAHA and increases the therapeutic safety window. This study clearly showed the promising potential of developing peptide hybrid for HDAC inhibition. We believe the peptide hybrid efficacy could be further enhanced by the discovery of more potent HDAC-binding peptides. Our findings also indicated that the cyclic peptides could inactivate HDACs and disrupt the LSD1-CoREST-HDAC1 interactions (Fig. 3; Supplementary Figs. S16A–S16B and S19A–S19B), which are reported to play a key role in cancer stem–like cells. Moreover, these peptides can also alter the properties of cancer stem–like cells by downregulating the stemness gene *Sox2*, upregulating the differential gene *FOXA2* and inducing caspase-3-dependent apoptosis and cell-cycle arrest (Figs. 3 and 4). Besides, our designed peptides could influence the proliferation of cancer stem–like cells *in vivo* with negligible organ lesions (Fig. 6). All these results indicated the great potential of our designed peptides for cancer therapy.

This proof-of-principle study has clearly shown the tremendous opportunity for the development of peptide/small-molecule hybrids to improve the safety window of these therapies, an application that could be applied for other important targets with similar needs. We also believe that with further understanding of the structurally based interaction between HDACs and their specific substrates, establishment of isoform-selective HDAC inhibitors could be realized.

Disclosure of Potential Conflicts of Interest

No potential conflicts of interest were disclosed.

Authors' Contributions

Conception and design: D. Wang, W. Liang, F. Yin, Z. Li
Development of methodology: D. Wang, W. Liang, F. Yin
Acquisition of data (provided animals, acquired and managed patients, provided facilities, etc.): D. Wang, W. Li, R. Zhao, L. Chen, N. Liu, M. Xie, Q. Fang
Analysis and interpretation of data (e.g., statistical analysis, biostatistics, computational analysis): D. Wang, Y. Tian, H. Zhao, F. Lu, W. Liang, F. Yin, Z. Li
Writing, review, and/or revision of the manuscript: D. Wang, W. Liang, F. Yin, Z. Li
Administrative, technical, or material support (i.e., reporting or organizing data, constructing databases): D. Wang, W. Liang, F. Yin, Z. Li
Study supervision: W. Liang, F. Yin, Z. Li

Acknowledgments

We acknowledge financial support from the Natural Science Foundation of China grants 21778009 (Z. Li), 81701818 (F. Yin), and 81572198 (Z. Li COPled); the Shenzhen Science and Technology Innovation Committee, JCYJ20170412150609690 (F. Yin), KQJSCX20170728101942700 (Z. Li), and

Downloaded from cancerres.aacrjournals.org on August 7, 2019. © 2019 American Association for Cancer Research.

Published OnlineFirst March 6, 2019; DOI: 10.1158/0008-5472.CAN-18-1421

JCYJ20170807144449135 (F. Yin COPled). This work is supported by the High-Performance Computing Platform of Peking University.

The costs of publication of this article were defrayed in part by the payment of page charges. This article must therefore be hereby marked *advertisement* in accordance with 18 U.S.C. Section 1734 solely to indicate this fact.

Received May 8, 2018; revised October 25, 2018; accepted February 28, 2019; published first March 6, 2019.

References

1. Hanahan D, Weinberg RA. Hallmarks of cancer: the next generation. Cell 2011;144:646–74.
2. Delude C. Tumorigenesis: testing ground for cancer stem cells. Nature 2011;480:S43–45.
3. Al-Hajj M, Wicha MS, Benito-Hernandez A, Morrison SJ, Clarke MF. Prospective identification of tumorigenic breast cancer cells. Proc Natl Acad Sci U S A 2003;100:3983–8.
4. O'Brien CA, Pollett A, Gallinger S, Dick JE. A human colon cancer cell capable of initiating tumour growth in immunodeficient mice. Nature 2007;445:106–10.
5. Peng S, Maihle NJ, Huang Y. Pluripotency factors Lin28 and Oct4 identify a sub-population of stem cell-like cells in ovarian cancer. Oncogene 2010;29:2153–9.
6. Li X, Wang J, Xu Z, Ahmad A, Li E, Wang Y, et al. Expression of Sox2 and Oct4 and their clinical significance in human non-small-cell lung cancer. Int J Mol Sci 2012;13:7663–75.
7. Witt AE, Lee CW, Lee TI, Azzam DJ, Wang B, Caslini C, et al. Identification of a cancer stem cell-specific function for the histone deacetylases, HDAC1 and HDAC7, in breast and ovarian cancer. Oncogene 2017;36:1707–20.
8. Liu C, Liu L, Shan J, Shen J, Xu Y, Zhang Q, et al. Histone deacetylase 3 participates in self-renewal of liver cancer stem cells through histone modification. Cancer Lett 2013;339:60–9.
9. Debeb BG, Lacerda L, Xu W, Larson R, Solley T, Atkinson R, et al. Histone deacetylase inhibitors stimulate dedifferentiation of human breast cancer cells through WNT/beta-catenin signaling. Stem Cells 2012;30:2366–77.
10. Fraga MF, Ballestar E, Villar-Garea A, Boix-Chornet M, Espada J, Schotta G, et al. Loss of acetylation at Lys16 and trimethylation at Lys20 of histone H4 is a common hallmark of human cancer. Nat Genet 2005;37:391–400.
11. Witt O, Deubzer HE, Milde T, Oehme I. HDAC family: What are the cancer relevant targets? Cancer Lett 2009;277:8–21.
12. Guha M. HDAC inhibitors still need a home run, despite recent approval. Nat Rev Drug Discov 2015;14:226–7.
13. Gregoretti IV, Lee YM, Goodson HV. Molecular evolution of the histone deacetylase family: functional implications of phylogenetic analysis. J Mol Biol 2004;338:17–31.
14. Seto E, Yoshida M. Erasers of histone acetylation: the histone deacetylase enzymes. Cold Spring Harb Perspect Biol 2014;6:a018713.
15. Yin F, Lan R, Zhang X, Zhu L, Chen F, Xu Z, et al. LSD1 regulates pluripotency of embryonic stem/carcinoma cells through histone deacetylase 1-mediated deacetylation of histone H4 at lysine 16. Mol Cell Biol 2014;34:158–79.
16. Kuzmochka C, Abdou HS, Hache RJG, Atlas E. Inactivation of histone deacetylase 1 (HDAC1) but not HDAC2 is required for the glucocorticoid-dependent CCAAT/enhancer-binding protein alpha (C/EBP alpha) expression and preadipocyte differentiation. Endocrinology 2014;155:4762–73.
17. Luo JY, Su F, Chen DL, Shiloh A, Gu W. Deacetylation of p53 modulates its effect on cell growth and apoptosis. Nature 2000;408:377–81.
18. Vaziri H, Dessain SK, Ng Eaton E, Imai SI, Frye RA, Pandita TK, et al. hSIR2 (SIRT1) functions as an NAD-dependent p53 deacetylase. Cell 2001;107:149–59.
19. Hubbert C, Guardiola A, Shao R, Kawaguchi Y, Ito A, Nixon A, et al. HDAC6 is a microtubule-associated deacetylase. Nature 2002;417:455–8.
20. Harrison SJ, Bishton M, Bates SE, Grant S, Piekarz RL, Johnstone RW, et al. A focus on the preclinical development and clinical status of the histone deacetylase inhibitor, romidepsin (depsipeptide, Istodax (R)). Epigenomics 2012;4:571–89.
21. Furumai R, Matsuyama A, Kobashi N, Lee KH, Nishiyama M, Nakajima H, et al. FK228 (depsipeptide) as a natural prodrug that inhibits class I histone deacetylases. Cancer Res 2002;62:4916–21.
22. Deschamps N, Simoes-Pires CA, Carrupt PA, Nurisso A. How the flexibility of human histone deacetylases influences ligand binding: an overview. Drug Discov Today 2015;20:736–42.
23. Zhao H, Liu QS, Geng H, Tian Y, Cheng M, Jiang YH, et al. Crosslinked aspartic acids as helix-nucleating templates. Angew Chem Int Edit 2016;55:12088–93.
24. Hu K, Geng H, Zhang Q, Liu Q, Xie M, Sun C, et al. An in-tether chiral center modulates the helicity, cell permeability, and target binding affinity of a peptide. Angew Chem Int Edit 2016;55:8013–7.
25. Jiang Y, Deng Q, Zhao H, Xie M, Chen L, Yin F, et al. Development of stabilized peptide-based PROTACs against estrogen receptor alpha. ACS Chem Biol 2018;13:628–35.
26. Hu K, Yin F, Yu M, Sun C, Li J, Liang Y, et al. In-tether chiral center induced helical peptide modulators target p53-MDM2/MDMX and inhibit tumor growth in stem-like cancer cell. Theranostics 2018;8:5660–1.
27. Watson PJ, Millard CJ, Riley AM, Robertson NS, Wright LC, Godage HY, et al. Insights into the activation mechanism of class I HDAC complexes by inositol phosphates. Nat Commun 2016;7:11262.
28. Xie W, Song C, Young NL, Sperling AS, Xu F, Sridharan R, et al. Histone H3 lysine 56 acetylation is linked to the core transcriptional network in human embryonic stem cells. Mol Cell 2009;33:417–27.
29. Du L, Risinger AL, King JB, Powell DR, Cichewicz RH. A potent HDAC inhibitor, 1-alaninechlamydocin, from a Tolypocladium sp induces G_2–M cell cycle arrest and apoptosis in MIA PaCa-2 cells. J Nat Prod 2014;77:1753–7.
30. Dehmel F, Weinbrenner S, Julius H, Ciossek T, Maier T, Stengel T, et al. Trithiocarbonates as a novel class of HDAC inhibitors: SAR studies, isoenzyme selectivity, and pharmacological profiles. J Med Chem 2008;51:3985–4001.
31. Yang F, Zhang T, Wu H, Yang Y, Liu N, Chen A, et al. Design and optimization of novel hydroxamate-based histone deacetylase inhibitors of Bis-substituted aromatic amides bearing potent activities against tumor growth and metastasis. J Med Chem 2014;57:9357–69.
32. Brooks H, Lebleu B, Vives E. Tat peptide-mediated cellular delivery: back to basics. Adv Drug Deliver Rev 2005;57:559–77.
33. Bird GH, Mazzola E, Opoku-Nsiah K, Lammert MA, Godes M, Neuberg DS, et al. Biophysical determinants for cellular uptake of hydrocarbon-stapled peptide helices. Nat Chem Biol 2016;12:845–52.
34. Rodrigues M, Andreu D, Santos NC. Uptake and cellular distribution of nucleolar targeting peptides (NrTPs) in different cell types. Biopolymers 2015;104:101–9.
35. Wang J, Lu F, Ren Q, Sun H, Xu Z, Lan R, et al. Novel histone demethylase LSD1 inhibitors selectively target cancer cells with pluripotent stem cell properties. Cancer Res 2011;71:7238–49.
36. Zhang X, Lu F, Wang J, Yin F, Xu Z, Qi D, et al. Pluripotent stem cell protein Sox2 confers sensitivity to LSD1 inhibition in cancer cells. Cell Rep 2013;5:445–57.
37. Qi D, Wang Q, Yu M, Lan R, Li S, Lu F. Mitotic phosphorylation of SOX2 mediated by Aurora kinase A is critical for the stem-cell like cell maintenance in PA-1 cells. Cell Cycle 2016;15:2009–18.
38. Kalin JH, Wu M, Gomez AV, Song Y, Das J, Hayward D, et al. Targeting the CoREST complex with dual histone deacetylase and demethylase inhibitors. Nat Commun 2018;9:53.
39. Gui CY, Ngo L, Xu WS, Richon VM, Marks PA. Histone deacetylase (HDAC) inhibitor activation of p21(WAF1) involves changes in promoter-associated proteins, including HDAC1. Proc Natl Acad Sci U S A 2004;101:1241–6.

Downloaded from cancerres.aacrjournals.org on August 7, 2019. © 2019 American Association for Cancer Research.

Published OnlineFirst March 6, 2019; DOI: 10.1158/0008-5472.CAN-18-1421

40. Li YX, Seto E. HDACs and HDAC inhibitors in cancer development and therapy. Cold Spring Harb Perspect Med 2016;6. pii: a026831. doi: 10.1101/cshperspect.a026831.
41. Wang YH, Wang CH, Jiang CG, Zeng H, He XJ. Novel mechanism of harmaline on inducing G2/M cell cycle arrest and apoptosis by up-regulating Fas/FasL in SGC-7901 cells. Sci Rep 2015;5:18613.
42. Dilworth D, Gudavicius G, Xu X, Boyce AKJ, O'Sullivan C, Serpa JJ, et al. The prolyl isomerase FKBP25 regulates microtubule polymerization impacting cell cycle progression and genomic stability. Nucleic Acids Res 2018;46: 2459–78.
43. Lao BB, Grishagin I, Mesallati H, Brewer TF, Olenyuk BZ, Arora PS, et al. In vivo modulation of hypoxia-inducible signaling by topographical helix mimetics. Proc Natl Acad Sci U S A 2014;111:7531–6.
44. Ding L, Zhang Z, Liang G, Yao Z, Wu H, Wang B, et al. SAHA triggered MET activation contributes to SAHA tolerance in solid cancer cells. Cancer Lett 2015;356:828–36.
45. Cai YY, Yap CW, Wang Z, Ho PC, Chan SY, Ng KY, et al. Solubilization of vorinostat by cyclodextrins. J Clin Pharm Ther 2010;35:521–6.
46. Jin Y, Yao Y, Chen L, Zhu X, Jin B, Shen Y, et al. Depletion of gamma-catenin by histone deacetylase inhibition confers elimination of CML stem cells in combination with imatinib. Theranostics 2016;6: 1947–62.
47. Mazur PK, Herner A, Mello SS, Wirth M, Hausmann S, Sánchez-Rivera FJ, et al. Combined inhibition of BET family proteins and histone deacetylases as a potential epigenetics-based therapy for pancreatic ductal adenocarcinoma. Nat Med 2015;21:1163–71.

Downloaded from cancerres.aacrjournals.org on August 7, 2019. © 2019 American Association for Cancer Research.

Published OnlineFirst March 6, 2019; DOI: 10.1158/0008-5472.CAN-18-1421

Cancer Research
The Journal of Cancer Research (1916–1930) | The American Journal of Cancer (1931–1940)

AACR American Association for Cancer Research

Stabilized Peptide HDAC Inhibitors Derived from HDAC1 Substrate H3K56 for the Treatment of Cancer Stem–Like Cells *In Vivo*

Dongyuan Wang, Wenjun Li, Rongtong Zhao, et al.

Cancer Res 2019;79:1769-1783. Published OnlineFirst March 6, 2019.

Updated version	Access the most recent version of this article at: doi:10.1158/0008-5472.CAN-18-1421
Supplementary Material	Access the most recent supplemental material at: http://cancerres.aacrjournals.org/content/suppl/2019/03/06/0008-5472.CAN-18-1421.DC1

Visual Overview	**A diagrammatic summary of the major findings and biological implications:** http://cancerres.aacrjournals.org/content/79/8/1769/F1.large.jpg

Cited articles	This article cites 46 articles, 7 of which you can access for free at: http://cancerres.aacrjournals.org/content/79/8/1769.full#ref-list-1

E-mail alerts	Sign up to receive free email-alerts related to this article or journal.
Reprints and Subscriptions	To order reprints of this article or to subscribe to the journal, contact the AACR Publications Department at pubs@aacr.org.
Permissions	To request permission to re-use all or part of this article, use this link http://cancerres.aacrjournals.org/content/79/8/1769. Click on "Request Permissions" which will take you to the Copyright Clearance Center's (CCC) Rightslink site.

Downloaded from cancerres.aacrjournals.org on August 7, 2019. © 2019 American Association for Cancer Research.